

Title: Explaining Indian Stock Market through Geometry of Scale free

Networks.

Pawanesh Yadav^{1, *#a}, Charu Sharma^{1, #a} and Niteesh Sahni^{1, #a}

¹Department of Mathematics, Shiv Nadar Institution of Eminence Deemed to be University,
Gautam Buddha Nagar, Uttar Pradesh, India

^{#a}Current Address: Department of Mathematics, Shiv Nadar Institution of Eminence Deemed
to be University, Gautam Buddha Nagar, Uttar Pradesh, India

*Corresponding Author

E-mail: py506@snu.edu.in

Phone: +91-9910056927

Abstract

This paper presents an analysis of the Indian stock market using a method based on embedding the network in a hyperbolic space using Machine learning techniques. We claim novelty on four counts. First, it is demonstrated that the hyperbolic clusters resemble the topological network communities more closely than the Euclidean clusters. Second, we are able to clearly distinguish between periods of market stability and volatility through a statistical analysis of hyperbolic distance and hyperbolic shortest path distance corresponding to the embedded network. Third, we demonstrate that using the modularity of the embedded network significant market changes can be spotted early. Lastly, the coalescent embedding is able to segregate the certain market sectors thereby underscoring its natural clustering ability.

Keywords : Complex network, Hyperbolic geometry, Machine learning.

1). Introduction

In the recent past, complex networks have emerged as a powerful tool to answer many fundamental questions about the stock market. Several authors have incorporated pairwise correlations between the rate of returns of stocks to model the pairwise interactions and constructed the networks [1-11]. Other popular choices of capturing the interaction between pairs of stocks have been the Kendall's tau [2], and Mutual information [3,4]. A large body of literature exploits the topology of financial networks [1-11] but very few have investigated the geometry of such networks. Only a handful of work with the financial networks embedded in Euclidean space [11,12]. Hyperbolic spaces have been shown to provide a more accurate representation of many topological-world networks than Euclidean spaces [13-17].

In fact, very recently in 2021 Ressel and Nargang [13] studied the latent geometry corresponding to the networks of European banks for the various years by embedding the underlying networks of banks in the Poincare disk. The vertices in the network were the banks and the weights associated with each edge was the liquidity-weighted portfolio overlap of one bank with the other bank. It measures the impact of sudden liquidation of portfolio of one bank on the other bank and vice versa. After embedding, each bank is assigned a radial coordinate r and an angular coordinate θ . Statistical methods are employed to establish associations between the radial coordinates and the systemic importance of the banks (known from the FSB reports) and also between the angular coordinates and regional sub sectors.

In reference [14], authors have an empirical evidence that the world trade network obey the power-law, that is they are heterogeneous. Based on this evidence, they drew inspiration from [20] and consequently adopted the connectivity probability while following the steps outlined in the referenced paper's proof to derive the radial and angular coordinates for each vertices in the Poincare disc.

A recently developed machine learning based algorithm of coalescent embedding provides a computationally effective and accurate means to embed complex network into a two dimensional or a three-dimensional hyperbolic space [15]. Coalescent embedding has been applied successfully to segregate different parts of the human brain from the MRI data [16]. The edges in the underlying networks were guided by the well-known anatomy of the human brain and certain pre-defined regions of the brain are treated as vertices of the network. The weight of each edge is chosen to be either the number of streamlines or the streamline distance between pairs of regions reported by Diffusion Tensor Imaging. Thus the edges are defined purely on the basis of anatomy rather than defined on the basis of a mathematical rule. It has been established that the regions of the brain (vertices) belonging to different lobes of the brain are clearly separated in the Poincare disc.

In this paper, we show that the Poincare disc [21] is a natural framework to study the Indian stock market and by leveraging community detection on the Poincare disc we are able to segregate stocks of different sectors and discover important patterns within a sector. Further, we compute three geometric measures hyperbolic distance (HD) and hyperbolic shortest path distance (HSD) of embedded network and apply non parametric statistical tests to segregate the periods of volatility and stability of the markets.

The standard method of finding communities in a network is to use the classical algorithm of Newman [22]. These communities will be referred to as topological communities throughout this paper and the family of topological communities will be denoted by \mathcal{C}^{top} . In [11] the authors embed a network into a Euclidean space via a nonlinear dimensionality reduction algorithm such as Isomap (ISO) [23] and subsequently use k-means algorithm to compute clusters denoted as \mathcal{C}^{Euc} . Finally, the similarity between \mathcal{C}^{top} and \mathcal{C}^{Euc} is adjusted on the basis of the Normalised mutual Information (NMI) [24, 25]. In the present paper, we apply the hyperbolic version of k-means algorithm [26, 27] to the network embedded in the hyperbolic disc to obtain the clusters and call the clusters so obtained as the hyperbolic clusters and denote the family of hyperbolic clusters by \mathcal{C}^{hyp} . Further, we compare the clusters on the basis of the Normalised mutual Information (NMI) as well as Normalised mutual Information (AMI) [28]. It has been observed that $NMI(\mathcal{C}^{top}, \mathcal{C}^{hyp})$ (as well as $AMI(\mathcal{C}^{top}, \mathcal{C}^{hyp})$) is significantly improved than the $NMI(\mathcal{C}^{top}, \mathcal{C}^{Euc})$ (as well as $AMI(\mathcal{C}^{top}, \mathcal{C}^{Euc})$). Thus, the topological community structure matches the hyperbolic clusters far more significantly than the ones obtained upon Euclidean embedding.

We begin our analysis by modelling the stock market data as a complex network by considering pairwise correlations between stocks. It is worth noting that the full correlation-based network has a homogeneous degree distribution and hence does not obey the power law. Thus, we need to work with certain subgraphs of the full network. The Minimum Spanning Tree (MST), the

Planar Maximally Filtered Graph (PMFG), and the PMFG-based threshold network (PTN) have been popular network models studied in a huge body of research over the years [1-11]. We shall also resort to these structures as our starting point.

As mentioned in Preliminary Section, any network for which the degree distribution of the vertices follow the power law can be embedded in the hyperbolic disc. So we carry out statistical computations to verify the validity of the power law for each of our networks – MST, PMFG, and PTN.

Angular separation index (ASI) [29] measures how well the clusters corresponding to the communities are separated in the hyperbolic space. The ASI score is constructed on the basis of counting the number of vertices of other communities that lie between each pair of successive vertices of a given community. Random shuffling of angular coordinates is performed a large number of times to calculate an empirical distribution of the ASI and p -values are computed to judge the quality of the observed ASI.

The remaining part of the paper is structured into 5 sections. In section 2, we give a description of the data used in our analysis. In Section 3, we present a preliminary definitions and methods utilized in our study. In section 4, we give the methodology adopted in the various analysis undertaken. Section 5 provides a detailed discussion of results. Lastly, in the concluding section, we summarize our key observations and future implication of the work.

2). Data description

Our data comprises of daily closing prices of all 500 stocks listed on the CNX500 index of the National Stock Exchange (NSE) India from January 01, 2017, till December 31, 2021. This accounts for 1236 working days. We removed the records of 117 stocks on the account of missing data of prices. This leaves us with the complete data of 383 stocks. Next, we calculate the daily logarithmic returns $r_i(t) = \log(p_i(t + 1)) - \log(p_i(t))$. Here $p_i(t)$ stands for the

closing price of the i -th stock at day t . While doing this we remove the data corresponding to non-successive days (like Friday & Monday are separated by more than 1 day because of holidays in between so we ignore the log return for Monday and similarly there were other exceptions also because of bank holidays). This leaves us with 939 values of logarithmic returns corresponding to the above 383 stocks.

3). Preliminaries

The two-dimensional hyperbolic space \mathbb{H}^2 (or the Poincare disc) is represented by the interior of the Euclidean disc of unit radius:

$$\mathbb{H}^2 = \{(x, y) \in \mathbb{R}^2; x^2 + y^2 < 1\}. \quad (1)$$

The hyperbolic distance between the two points $x = (x_1, x_2)$ and $y = (y_1, y_2)$ in \mathbb{H}^2 is given by

$$d(x, y) = \cosh^{-1} \left(1 + \frac{2\|x - y\|^2}{(1 - \|x\|^2)(1 - \|y\|^2)} \right). \quad (2)$$

Alternatively, the hyperbolic distance x_{ij} between two points in the Poincare disc with polar coordinates (r, θ) and (r', θ') is given by

$$x_{ij} = \frac{1}{\zeta} \cosh^{-1} (\cosh(\zeta r) \cosh(\zeta r') - \sinh(\zeta r) \sinh(\zeta r') \cos \Delta \theta). \quad (3)$$

Where $\zeta = \sqrt{-K}$, K is curvature of the hyperbolic space and $\Delta \theta = \pi - |\pi - |\theta - \theta' ||$ is the angular distance between points. The hyperbolic distance equation 3 has the following well known approximation:

$$x_{ij} \approx r + r' + \frac{2}{\zeta} \ln \left(\frac{\Delta \theta}{2} \right). \quad (4)$$

The boundary $\partial \mathbb{H}^2$ of the disc is given by the circle, \mathbb{S}^1

$$\mathbb{S}^1 = \{(x, y) \in \mathbb{R}^2; x^2 + y^2 = 1\}.$$

The area and the circumference of the hyperbolic disc \mathbb{H}^2 can be given by

$$L(r) = 2\pi \sinh(\zeta r) \propto e^{\zeta r}.$$

$$A(r) = 2\pi(\cosh(\zeta r) - 1) \propto e^{\zeta r}.$$

Hyperbolic spaces are a natural framework for embedding scale free networks which we now explain.

Let the degree distribution of the vertices of the scale free network follow the power law $P(k) \propto k^{-\gamma}$. In order to embed this network in a Poincare disc, we start by uniformly distributing the N vertices on a circle of radius $R = \frac{N}{2\pi}$ and assign an angular coordinate θ to each vertex. Let κ stand for the expected degree of each vertex in the network. Now corresponding to each vertex we have a pair (κ, θ) . Treating κ as a hidden variable [30], we can write

$$P(k) = \int_{\kappa_0}^{\infty} g(k|\kappa)\rho(\kappa)d\kappa. \quad (5)$$

Here $g(k|\kappa) = \frac{e^{-\bar{k}(\kappa)}(\bar{k}(\kappa))^k}{k!}$ according to [31].

The probability that two vertices (κ, θ) and (κ', θ') are joined by an edge is $\tilde{p}(\chi)$, where χ is chosen in [20] as $\chi = \frac{d}{\mu\kappa\kappa'}$ where d is the arc length and the parameter $\mu > 0$.

Following [31], the average degree of vertices with expected degree κ is given by

$$\bar{k}(\kappa) = \frac{N}{2\pi} \int_{\kappa_0}^{\infty} \int_0^{2\pi} \rho(\kappa')\tilde{p}(\chi) d\kappa' d\theta'$$

and further it turns out that $\bar{k}(\kappa) = \kappa$.

Now, substituting $\rho(\kappa) = \kappa_0^{\gamma-1}(\gamma-1)\kappa^{-\gamma}$, where $\gamma > 2$ and $\kappa \geq \kappa_0$, and the expression for $g(k|\kappa)$ in equation 5 we get

$$P(k) = \int_{\kappa_0}^{\infty} \frac{e^{-\kappa}(\kappa)^k}{k!} \kappa_0^{\gamma-1}(\gamma-1)\kappa^{-\gamma} d\kappa$$

$$\begin{aligned}
&= \frac{\kappa_0^{\gamma-1}(\gamma-1)}{k!} \int_{\kappa_0}^{\infty} e^{-\kappa} (\kappa)^{k-\gamma+1-1} d\kappa \\
&= \frac{\kappa_0^{\gamma-1}(\gamma-1)}{k!} [\Gamma(k-\gamma+1, \kappa_0)]
\end{aligned}$$

Thus

$$P(k) \propto k^{-\gamma}.$$

Thus every scale free network of a given distribution can be generated by considering the distribution of the expected degree of each vertex.

We now map the point (κ, θ) to a point (r, θ) in the disc via the transformation:

$$r = R - \frac{2}{\zeta} \log\left(\frac{\kappa}{\kappa_0}\right) \quad (6)$$

(Note that $0 < r < R = 2\ln\left(\frac{N}{\mu\pi\kappa_0^2}\right)$)

As a consequence of the above transformation we also have

$$\rho(\kappa) = \rho\left(\kappa_0 e^{\frac{(R-r)\zeta}{2}}\right) = \kappa_0^{-1}(\gamma-1)e^{\frac{\gamma\zeta(r-R)}{2}} \propto e^{\frac{\gamma\zeta r}{2}} \quad (7)$$

and $\chi = e^{\frac{\zeta(x-R)}{2}}$, where x is the hyperbolic distance between two vertices. The vertices (r, θ) and (r', θ') are connected by an edge according to the connection probability $\tilde{p}(\chi) = H(1 - \chi)$. Also the role of the curvature of the hyperbolic space is played by $\frac{\gamma\zeta}{2}$.

On the other hand, a striking consequence of hyperbolic geometry is that N points distributed over the Poincare disc can be thought of as vertices of a network satisfying the power law. We explain this briefly as under.

Consider Poincare disc with radius R . Assume that the angular coordinates θ_i of the N points (r_i, θ_i) are from the uniform distribution $\rho(\theta) = \frac{1}{2\pi}$ on the interval $[0, 2\pi]$. The radial density is given by $\rho(r) = \frac{L(r)}{A(R)} \approx e^{r-R}$, $r \in [0, R]$. These N points constitute the vertex set $\{1, 2, \dots, N\}$ of the graph. Next, there will be an edge between vertices i and j if $x_{ij} \leq R$. In other words,

the connection probability function takes the form $p(x) = H(R - x)$, where $H(t)$ stands for the heaviside step function. It turns out that $P(k) \propto k^{-3}$. For details the reader refer to [20].

In this paper we shall work with embeddings of two kinds of sub-graphs: the Minimum spanning tree (MST) and the Planar maximally filtered graph (PMFG).

In MST we retain the most significant edges by defining the edge weight using the distance

$d_{ij} = \sqrt{2(1 - \rho_{ij})}$, where ρ_{ij} is the Pearson correlation between the log returns of the stock

i and stock j . Next, Prim's algorithm [32] is employed to find a spanning tree with minimum sum of the total edge weights. The importance of using d_{ij} as a weight has been highlighted in [1-11].

The PMFG subgraph of a graph $G = (V, E)$ with adjacency matrix $A = [a_{ij}]_{n \times n}$ is extracted

as follows: First, consider the upper triangular part of the matrix A and extract the $\frac{n(n-1)}{2}$

elements a_{ij} (this is the weight associated with the edge e_{ij}) and arrange them into a vector S

and sort S in descending order. Call the sorted list as S' . Initialize with the first six elements

from list S' and retain all the edges associated with the vertices corresponding to these 6

weights. Call this graph as PMFG. Note that PMFG is planar because it has six edges. Next,

continue to add the next element from list S' in the PMFG, if the tested PMFG graph is planar

(usually through Boyer-Myrvold algorithm [33]), else discard. According to Euler's theorem

[34], this continues till $3n - 6$ edges are included. When this process ends, we are left with a

maximally filtered planar graph. It is worth pointing out that the Boyer-Myrvold algorithm

implements two steps at its core: first, it creates a straight-line drawing of a planar graph by

mapping all n vertices to integer coordinates using an algorithm by Chrobak and Payne [35].

Second, it verifies that the result produced in the first to have a straight-line representation or not. This step uses the Fary's theorem [36].

A brief overview of the key procedures and statistical measures used throughout our analysis are presented in sections 3.1-3.5.

3.1). Validity of Power-law in networks

Let $P(k)$ stand for the probability that a randomly chosen vertex has k edges attached to it. A complex network is said to follow a power law if $P(k) \propto k^{-\gamma}$.

The parameter γ has a convenient approximation given in [37]:

$$\gamma \cong 1 + n \left(\sum_{i=1}^n \ln \left(\frac{d_i}{k_{min}-0.5} \right) \right)^{-1} \quad (8)$$

where d_i is the degree of the i^{th} vertex and k_{min} is the minimum degree. The Kolmogorov-Smirnov (KS) test [37] was employed to distinguish between the following hypothesis

H_0 : The degree distribution follows the power law distribution for $d \geq k_{min}$.

H_1 : The degree distribution does not follow the power law distribution for $d \geq k_{min}$.

A high p -value suggests a good power-law fit (with exponent γ) and a low p -value is indicative of a poor fit.

3.2). Fast Newman community detection algorithm

The classical fast Newman community algorithm [22] iteratively produces the partitions of the network vertices into communities and assesses the modularity Q at each iteration. We compute Q as follows:

$$Q = \sum_i (L_{ii} - a_i^2). \quad (9)$$

Here L_{ij} is the fraction of all edges that connect vertices of group i to those of group j , and $a_i = \sum_j L_{ij}$. The numbers L_{ij} and a_i depend on the edge weights.

The algorithm begins by treating the N vertices as one member communities. Next, consider all possible pairs of communities and compute the change in modularity given by $\Delta Q = L_{ij} + L_{ji} - 2a_i a_j$ for each pair. Now, merge the pair yielding the largest ΔQ . Continue this process till there is no significant increase in ΔQ .

In this paper we have applied the fast Newman algorithm to embedded networks in the Poincare disk by choosing the edge weight between vertices i and j suggested in [15, 38] as

$$w_{ij} = w_{ji} = \frac{1}{1+x_{ij}}. \quad (10)$$

Here x_{ij} is the hyperbolic distance between the vertices i and j as defined in section 3.

3.3). Coalescent embedding algorithm

Coalescent embedding is recent technique introduced in [15] and has non-linear dimensionality reduction at its core. The dimensionality reduction is usually accomplished through popular algorithms like Isomap (ISO) [23], Non-centred Isomap (ncISO), Laplacian eigenmaps (LE) [39], Minimum curvilinear embedding (MCE) and Non-centred minimum curvilinear embedding (ncMCE) [40, 41]. All these algorithms embed the weighted network (with weighted adjacency matrix W) into the d -dimensional Euclidean space. In this paper we choose the elements of W as $w_{ij} = \rho_{ij}$ if vertex i and j are adjacent; and 0 otherwise, and choose $d = 2$. The matrix W is of order $N \times N$ and so at this point, we have, for each vertex i , a pair of topological number (x_i, y_i) . So we can assign an angular coordinate $\theta_i = \tan^{-1} \left(\frac{y_i}{x_i} \right)$ corresponding to each vertex. These angular values are referred to as circular adjustment (CA). The equidistance adjustment (EA) for the i^{th} vertex is defined by

$$\theta_i' = \frac{2\pi}{N}(t_i - 1).$$

Here t_i is the rank assigned to the i^{th} vertex obtained after sorting the original angular coordinates in ascending order.

In order to assign the radial coordinate to each vertex in the network, the vertex degrees are sorted in descending order $d_1 \leq d_2 \leq \dots \leq d_N$ (i.e., highest degree vertices appearing first).

Then radial coordinate for each $i = 1, 2, \dots, N$ is chosen as:

$$r_i = \frac{2}{\zeta} [\beta \ln(i) + (1 - \beta) \ln(N)].$$

Thus, each vertex of the network can be represented by (r_i, θ_i) and the above expression of r_i forces each vertex to belong to the hyperbolic space. Also, in view of [42], the above transformation forces the embedded vertices to follow a power law with exponent $\beta = \frac{1}{\gamma-1} \in (0,1]$ as $2 < \gamma < 3$.

3.4). Embeddings into Euclidean Space of lower dimension

Assume that an observed data set $X = \{x_1, x_2, \dots, x_N\} \subseteq \mathbb{R}^D$ be a set of N data points lie on an unknown manifold $M \subseteq \mathbb{R}^D$. The goal is to project the data points onto a Euclidean space of dimension $d \ll D$ in a meaningful way. A general strategy to do this is suggested in [43] wherein a coordinate mapping $f: M \rightarrow \mathbb{R}^d$ preserving the geodesics distance is found. The set $Y = \{f(x_1), \dots, f(x_N)\}$ is the required low dimensional representation of X . In practice, the Isomap algorithm is a popular method for accomplishing this task [11, 23, 44].

3.5). Statistical Measures

In this section we briefly discuss two well-known statistics to capture the similarities between the clusters and the communities. The first two measures are Normalised Mutual Information

(NMI) and Adjusted mutual Information (AMI) introduced in [24, 25] and the third is the Angular separation index (ASI) introduced in [29]. The ASI is particularly useful to measure the separation between communities in the setting of Poincare disk since its formulation depends on the angular coordinates assigned to the vertices. To be precise the ASI score is computed between two “most distant” nodes in a given community. For precise details the reader may refer to [29]. Let the observed ASI be α . We repeat the calculation of the ASI for a large number of random shuffling of the angular coordinates of the vertices in the Poincare disc. Each shuffling yields a different ASI. So, calling ASI^k to be the computed ASI for the k^{th} shuffling we can empirically calculate the p -value to determine the statistical significance of the observed ASI. Mathematically this p -value is given by:

$$p = \frac{1 + \sum_k \delta(ASI^k \geq \alpha)}{1 + Z}$$

Where Z is the total number of shuffling and $\delta(x) = 1$, if $ASI^k \geq \alpha$ and $\delta(x) = 0$, if $ASI^k < \alpha$.

On the other hand, the NMI between two partitions $A = \{A_1, A_2, \dots, A_{N_1}\}$ and $B = \{B_1, B_2, \dots, B_{N_2}\}$ of the network is defined based on mutual information.

$$MI(A, B) = - \sum_{i=1}^{N_1} \sum_{j=1}^{N_2} M(i, j) \log \left(\frac{M(i, j)N}{r(M_i) \cdot c(M_j)} \right) \quad (11)$$

$$NMI(A, B) = \frac{-2 * \sum_{i=1}^{N_1} \sum_{j=1}^{N_2} M(i, j) \log \left(\frac{M(i, j)N}{r(M_i) \cdot c(M_j)} \right)}{\sum_{i=1}^{N_1} r(M_i) \log \left(\frac{r(M_i)}{N} \right) + \sum_{j=1}^{N_2} c(M_j) \log \left(\frac{c(M_j)}{N} \right)}. \quad (12)$$

Here $M(i, j)$ stands for the number of vertices common to A_i and B_j , and $r(M_i) = \sum_j M(i, j)$, $c(M_j) = \sum_i M(i, j)$ are row sum and column sum of the confusion matrix M , respectively.

Using the expected mutual information defined in [30], the adjusted mutual information for the shuffled network partitions A' , B' can be expressed as follows:

$$AMI(A, B) = \frac{MI(A, B) - E(MI(A', B'))}{\frac{1}{2} (\sum_{i=1}^{N_1} r(M_i) \log\left(\frac{r(M_i)}{N}\right) + \sum_{j=1}^{N_2} c(M_j) \log\left(\frac{c(M_j)}{N}\right)) - E(MI(A', B'))} \quad (13)$$

4). Methodology

Our findings establish the superiority of embedding the networks in a hyperbolic space (coalescent embedding) versus embedding same networks in the Euclidean space on the following four counts:

- Topological communities verses clusters of the embedded networks.
- Identifying the periods of the volatility and stability of the market.
- Modularity of embedded network – a tool to capture market sensitivity.
- Visualizing Market sectors through the coalescent embedding.

We elaborate on each of the above questions in sections 4.1-4.4 given below.

4.1). Topological communities verses clusters of the embedded networks

Step 1. Define a pairwise correlation-based network of stocks using the available time series data in the section 2.

We define a correlation based network represented by $G = (V, E)$ from the data where the set of vertices V consists of the 383 stocks and the weight assigned to each edge e_{ij} is the Pearson correlation coefficient ρ_{ij} given by

$$\rho_{ij} = \frac{E[r_i r_j] - E[r_i]E[r_j]}{\sqrt{E[r_i^2] - E[r_i]^2} \sqrt{E[r_j^2] - E[r_j]^2}}. \quad (13)$$

Here r_i and r_j is the corresponding log returns of stocks i and j , respectively. This construction is in the spirit of [1-10].

Step 2. Extract subgraphs by eliminating redundant edges to mitigate the effect of noise [1-12] and introduce heterogeneity in the complex system which will justify the embedding into the hyperbolic space according to preliminary section 3. The sub graphs that we worked with were the MST and the PMFG. The MST is extracted using the Prim's algorithm [32] and the PMFG was extracted using the procedure outlined in preliminary section.

- We carried out the community analysis using the fast Newman algorithm [22].
- The communities extracted in the previous step will be referred to as topological communities and the collection of all topological communities is denoted by C^{top} .

Step 3. Using the procedure outlined in section 3.1, the validity of the power law was examined for the MST, PMFG and PTN subgraphs. In case of MST (obtained from the full correlation network) we choose $k_{min} = 2$ and choose $k_{min} = 3$ in case of PMFG. High p -values (> 0.1) in both cases indicate the presence of power law distribution. However no conclusive evidence of power law distribution was seen in case of PTN subgraphs and hence we discard PTN altogether from our further analysis. The respective estimates of γ and the p -values for the MST, PMFG and PTN networks corresponding yearly data is provided in the supporting information (S1 Table). It has also been observed (by repeating the hypothesis test on yearly data) that the networks constructed from 60 day windows also follow the Power law distribution. For the sake of brevity we present the results for MST only in this paper and relegate those of PMFG in the supporting information since the conclusions are very similar.

Step 4. Carry out the coalescent embedding for the corresponding sub graphs (obtained in step 2) to embed them in Poincare disc. This identifies each vertex i of the graph with a pair of numbers (r_i, θ_i) as described in section 3.3.

- Compute the clusters in the Poincare disc using the hyperbolic version of k-means and referred as C^{hyp} .

Step 5. Similarly to step 4, carry out the Euclidean embeddings for the corresponding sub graphs (obtained in step 2). This identifies each vertex i of the graph with a pair of numbers (x_i, y_i) in Euclidean plane as described in section 3.4.

- Compute the clusters in the Euclidean space using k-means and referred as C^{euc} .

Step 6. Compare the quality of topological communities with the low dimensional Euclidean clusters and hyperbolic clusters on the basis of NMI (or AMI) score.

4.2). Identifying the periods of the volatility and stability of the market

Step 1. To evaluate the geometrical changes in the stock networks subject to two different Market conditions (Healthy period and crisis period), we selected two specific years data among the five years data. For the healthy period we selected year 2018 characterized by lowest standard deviation and for the crisis period year 2020 characterized by highest standard deviation. The Table 1. reports the price statistics for both the specified periods data. Fig 1 depicts the market price trend of the CNX100 Index for healthy and crisis periods.

Here first we list below in Table 2. some of the network topological properties such as average edge weight (EW) , average weighted mean degree (MD) (twice of EW), average shortest path distance(SD) and average local clustering coefficient (CC) of the MST networks constructed on whole year datasets of both periods and corresponding Table for PMFG Network provided in the supplementary information (S2 Table).

Step 2. Following the step 1 to 4 of section 4.1, we, generate the series of correlation-based networks (MST, PMFG) with the calculation window for 60 days and the sliding window for 1 day over both periods. So, the total number of windows were 137 and 124 in Year 2020 and

Year 2018, respectively. Next, we embedded of the generated network in the Poincare disc via various class of the coalescent embedding algorithm. Further, for each of the class of the coalescent embedding, we compute the numbers HD (equation 3) and HSD for each of the underlying network for different time spans that corresponds to healthy and crisis period. Along with this we also compute the average edge weight each of the original MST and PMFG networks of the both the periods. Computation of HSD involves finding the shortest path between pairs of vertices (usually by Dijkstra's algorithm [41]) with edge weights chosen to be the hyperbolic distance between the vertices and then summing up the edge weights.

Step 3. Further, carry out the Mann Whitney test [42] on the two population of HD of both the periods (Healthy and crisis) and similarly on the HSD. We also perform the Mann Whitney test on the average edge weight of the MST and PMFG networks of the both the periods.

Step 4. Periods were distinguished on the basis of p -value with significance level 0.05.

4.3). Modularity of embedded network – a tool to capture market sensitivity.

Step 1. Similar to step 1 refer in section 4.2, we generate the series of correlation-based MST networks with the calculation window for 60 days and the sliding window for 1 day over the five years dataset. There were total 879 windows.

Step 2. We carried out the community analysis as described in step 2 of section 4.1 for each of above 879 networks and collect the maximum modularity obtained for each of the network communities. We refer this modularity as original modularity.

Step 3. Next, we carry out the step 4 of section 4.1 over each of the 879 networks and identify each node i as a polar coordinate form (r_i, θ_i) as described in section 3.3.

- Repeat the computation of communities in the embedded network. Collect the maximum modularity obtained for each of the 879 network communities and refer as the hyperbolic modularity.

Step 4. Now setup two time series $\{O_t\}_t$, and $\{H_t\}_t$ as original modularity of the original network and the hyperbolic modularity of the embedded network (after applying coalescent embedding to corresponding MST (or PMFG)) respectively.

Step 5. We compute the Simple moving average (SMA) time series for O_t and H_t for $N = 20$ days as follows: $O'_t = \frac{1}{20} \sum_{j=0}^{19} O_{t-j}$ and $H'_t = \frac{1}{20} \sum_{j=0}^{19} H_{t-j}$. The Bollinger Bands (BB) [47] of O'_t and H'_t calculated as $[O'_t - 3\sigma_t^O, O'_t + 3\sigma_t^O]$, and $[H'_t - 3\sigma_t^H, H'_t + 3\sigma_t^H]$. In the corresponding intervals the series $O'_t - 3\sigma_t^O$ and $H'_t - 3\sigma_t^H$ are called lower Bollinger Band referred as lowerBB, similarly the series $O'_t + 3\sigma_t^O$ and $H'_t + 3\sigma_t^H$ are called upper Bollinger Band referred as upperBB. Here σ_t^O and σ_t^H stand for the standard deviations time series for O_t and H_t . For the sake of comparison, we repeat the above BB calculations for the time series of prices $\{P_t\}_t$ over the same five years period. We present the inferences drawn on the basis of the above analysis in section 5.3.

4.4). Visualising Market sectors through the coalescent embedding

Step 1. Following the steps 1 to 4 of section 4.1, we visualise certain market sectors via coalescent embedding in Poincare disc. For this we selected stocks over five-years 2017 to 2021 from the sectors: (i) Finance (ii) Healthcare (iii) Information Technology.

Step 2. We create the visualisation of MST networks in the Poincare disc corresponding to finance, healthcare sectors and all three sectors, respectively.

Step 3. A quantitatively separation of topological communities performed on the basis of ASI score (section 3.5) has been performed in the Poincare disc.

5). Results

5.1). Topological communities verses clusters of the embedded networks

This analysis is performed on yearly dataset. First, we employed the classical Newman community detection algorithm to extract the topological communities (\mathcal{C}^{top}) of each network. Further, we used various non-linear dimension reduction techniques (ISO, ncISO, LE, MCE and ncMCE) to embed these networks into the Euclidean plane and computes the clusters \mathcal{C}^{Euc} using k-means. Next, we calculate the NMI (or AMI) score between \mathcal{C}^{top} and \mathcal{C}^{Euc} . We also embedded each network in Poincare disc via various classes of the coalescent embedding and extracted the hyperbolic k-means clusters \mathcal{C}^{hyp} . Next, calculate the NMI (or AMI) score between the \mathcal{C}^{top} and \mathcal{C}^{hyp} . Table 3 and Table 4 reports the NMI and AMI score, respectively. We observe that the NMI (or AMI) score between the \mathcal{C}^{top} and \mathcal{C}^{hyp} is bit improved in three classes of coalescent embedding (ncISO, LE, ncMCE) than the NMI (or AMI) score between the \mathcal{C}^{top} and \mathcal{C}^{Euc} (MST Network) of the respective Euclidean embeddings. LE-EA class of the coalescent embedding has the best NMI (or AMI) score consistently over the years in comparison to other classes. Note that the Minimum score of $NMI(\mathcal{C}^{top}, \mathcal{C}^{hyp})$ is 0.579 while the maximum score of $NMI(\mathcal{C}^{top}, \mathcal{C}^{hyp})$ is 0.854. Thus, we conclude that the coalescent embedding outperforms the respective three Euclidean methods (ncISO, LE, ncMCE) in term of the NMI (or AMI) score. Similar, results are observed for the PMFG networks in the supplementary information (S3 Table (a) and (b)). An example of embedding the topological

communities in the Euclidean plane and the hyperbolic disc is given in Fig 2 for the MST network corresponding to year 2017 data.

Further, we also performed the MW test over the two NMI series (generated using the step 1 of section 4.3 and then carry out step 2 to step 6 of the section 4.1) denoted as NMI_{top}^{Euc} corresponding to the Euclidean methods (i.e., ISO, ncISO, LE, MCE, ncMCE) and NMI_{top}^{hyp} its corresponding hyperbolic embedding methods (i.e., ISO-EA, ncISO-EA, LE-EA, MCE-EA, ncMCE-EA). Next, we use the Man-Whitney test over these NMI series and test the hypothesis:

$$H_0: \text{mean}(NMI_{top}^{hyp}) < \text{mean}(NMI_{top}^{Euc})$$

$$H_1: \text{mean}(NMI_{top}^{hyp}) \geq \text{mean}(NMI_{top}^{Euc})$$

We show below in Table 5 and we conclude that mean of NMI_{top}^{hyp} values were greater than mean of NMI_{top}^{Euc} over the five years for methods ncISO, LE, ncMCE. So We can say that on the basis of statistical analysis for these three methods their corresponding hyperbolic coalescent embedding methods matches topological communities more closely with hyperbolic clusters than Euclidean methods. Almost, similar results are observed in the PMFG network provided in supplementary information (S4 Table).

5.2). Identifying the periods of the volatility and stability of the market

As explained in the section 4.2 step 2, each of the network (year 2018 and year 2020) has been embedded into Poincare disc using the coalescent embedding algorithm. Next, we calculated mean of each geometrical measures HD and HSD. Table 6 reports, for each method (EA and CA), the mean measure of the two groups, the p -values of the Mann-Whitney test. For

reference, we also compute the mean of all four measures listed in table 2, such as MD, SD, EW and CC of the original networks. Here we report only in the SD and EW (because their mean of crisis period greater than the healthy period) for both the periods. Below we provided in Fig. 4 and Fig. 5 the probability distributions of measures (SD, EW, HD and HSD) plotted as histogram corresponding to MST networks of both the periods, respectively and for PMFG provided in the supplementary information (S1 Fig (a) and (b)). Note that in Table 6, for the case SD measure of original network, p -value is quite significant at 0.05 level of confidence, but not in the case of EW measure. On the other hand, Note that p -values for all the classes of coalescent embedding methods are significant at 0.05 level of confidence and even equal to zero in some cases, which indicates that the Mann Witney test on SD measure is also able to segregate the both periods but hyperbolic measures HD and HSD are able to segregate more effectively. Similar, results are observed for the PMFG networks in the supplementary information (S5 Table).

5.3). Modularity of embedded network – a tool to capture market sensitivity

In Fig 5, Fig 6 and Fig 7 we observe that the SMA series of the hyperbolic modularity (Corresponding to ISO-CA class of Coalescent embedding algorithm) crosses its respective lowerBB even before the SMA series of the original modularity and the prices series crosses their respective lowerBB. For example the first time SMA series of hyperbolic modularity crosses its lowerBB at tick 14 (date 28/06/17) before the crossover of the SMA series of the original modularity at tick 52 (date 07/09/17) and the prices series at the tick 188 (date 23/05/18). With this we conclude that the hyperbolic modularity is more sensitive to the market events, crisis or fluctuation in compared to original network modularity and captures the market trend even before captured by the original modularity. As a result, financial investor can

monitor the hyperbolic modularity as an early indicator of the market movement and potential trading opportunities in future.

We also performed the one tailed Mann Whitney test in order to test the hypothesis that

$$H_0: \mu_H < \mu_O$$

$$H_A: \mu_H \geq \mu_O$$

Where μ_H is the mean of the hyperbolic modularity and the μ_O is the mean of the original modularity. The one tailed Mann Whitney test produces the p -value close to 0, which means that we reject the null hypothesis and accept the alternative hypothesis. This implies that the mean of the hyperbolic modularity is greater than the mean of the original modularity.

5.4). Visualising Market sectors through the coalescent embedding

Co-movement of stocks have been studied in the literature using techniques like Multidimensional scaling dimensionality reduction [12], Dendrogram and MST methods [12], and Random Matrix Theory [3]. Local network indices have also been a popular tool to analyse co-movement of stocks. For this, we have selected stocks over the five-years 2017 to 2021 from three sectors: (i) Finance (ii) Healthcare (iii) Information Technology. We embedded the MST network corresponding to the stocks in Finance and Healthcare sector in Fig 8 and also corresponding stocks on all three sectors Finance, Healthcare and Information technology in Fig 9. It is quite evident that coalescent embedding visually is able to segregates sectors clearly.

The separation of topological communities quantitatively on the basis of ASI has been performed in the hyperbolic disc. Table 7 gives the ASI scores showing the degree of separation of topological communities of MST network in the 2D hyperbolic Space in the context of various embedding algorithms and years. A score close to 1 (p -value < 0.001) indicate the successful separation of topological communities. The result clearly indicates that all the classes of the coalescent embedding methods are able to segregate the topological communities in the hyperbolic space with LE-EA showing the best results. For all the methods, we note that the observe p -values are close to 0.00099. Similar, results are observed for the PMFG networks in the supplementary information (S6 Table).

Conclusion

In this study, we consider the Poincare disc as a natural framework to explore the Indian stock market and demonstrate the use of the hyperbolic geometry underlying the subnetworks (MST, PMFG) of the full correlation-based network. The paper comprehensively explores the community structure of the networks and compares it with the clusters obtained after embedding the networks in the Euclidean space and hyperbolic space using NMI (or AMI) scores. Results shows that some classes of the coalescent embedding (ncISO, LE, ncMCE) outperforms the respective Euclidean embeddings methods. Also, the analysis based on the ASI scores showed that the coalescent embedding effectively segregates the topological communities in the hyperbolic space. The analysis also supports the natural clustering property of the coalescent embedding with the sectoral co-movement. Next, we showed that the hyperbolic modularity has ability to spot a significant change in the market. This research also demonstrates the use of parameters HD and HSD in order to effectively differentiate between periods of market stability and volatility. In summary, this research amalgamates financial analysis, network science, hyperbolic geometry, and Machine learning to shed new and

illuminating insights on the dynamics of the Indian stock market. It introduces an innovative approach that effectively distinguishes market volatility from stability, enabling the early detection of market shifts. Furthermore, it showcases the superior performance of hyperbolic embedding in comprehending complex financial systems. In future, the hyperbolic clusters can be leveraged to create new portfolios and it would be interesting to analyse their properties in terms of rate of return and risk.

Acknowledgement

We thank the Shiv Nadar Institution of Eminence for providing the computational facilities and the necessary infrastructure needed to carry out the present research. We extend a special gratitude to Professor Sanjeev Agrawal for his encouragement and valuable comments.

References

- [1] Jiang XF, Chen TT, Zheng B. Structure of local interactions in complex financial dynamics. *Scientific reports*. 2014 Jun 17;4(1):5321. <https://doi.org/10.1038/srep05321>
- [2] Millington T, Niranjan M. Construction of minimum spanning trees from financial returns using rank correlation. *Physica A: Statistical Mechanics and its Applications*. 2021 Mar 15;566:125605. <https://doi.org/10.1016/j.physa.2020.125605>
- [3] Sharma C, Habib A. Mutual information based stock networks and portfolio selection for intraday traders using high frequency data: An Indian market case study. *PloS one*. 2019 Aug 29;14(8):e0221910. <https://doi.org/10.1371/journal.pone.0221910>
- [4] Guo X, Zhang H, Tian T. Development of stock correlation networks using mutual information and financial big data. *PloS one*. 2018 Apr 18;13(4):e0195941. <https://doi.org/10.1371/journal.pone.0195941>

- [5] Aste T, Shaw W, Di Matteo T. Correlation structure and dynamics in volatile markets. *New Journal of Physics*. 2010 Aug 19;12(8):085009. <https://doi.org/10.1088/1367-2630/12/8/085009>
- [6] Pozzi F, Di Matteo T, Aste T. Spread of risk across financial markets: better to invest in the peripheries. *Scientific reports*. 2013 Apr 16;3(1):1665. <https://doi.org/10.1038/srep01665>
- [7] Chi KT, Liu J, Lau FC. A network perspective of the stock market. *Journal of Empirical Finance*. 2010 Sep 1;17(4):659-67. <https://doi.org/10.1016/j.jempfin.2010.04.008>
- [8] Kumar S, Deo N. Correlation and network analysis of global financial indices. *Physical Review E*. 2012 Aug 2;86(2):026101. <https://doi.org/10.1103/PhysRevE.86.026101>
- [9] Hakeem MM, Ichi Suzuki K. Centrality measures for trade and investment networks. *Australian Academy of Accounting and Finance Review*. 2017 Feb 14;1(2):103-18.
- [10] Tumminello M, Aste T, Di Matteo T, Mantegna RN. A tool for filtering information in complex systems. *Proceedings of the National Academy of Sciences*. 2005 Jul 26;102(30):10421-6. <https://doi.org/10.1073/pnas.0500298102>
- [11] Nie CX, Song FT. Constructing financial network based on PMFG and threshold method. *Physica A: Statistical Mechanics and its Applications*. 2018 Apr 1;495:104-13. <https://doi.org/10.1016/j.physa.2017.12.037>
- [12] Sharma K, Shah S, Chakrabarti AS, Chakraborti A. Sectoral co-movements in the Indian stock market: a mesoscopic network analysis. *Economic Foundations for Social Complexity Science: Theory, Sentiments, and Empirical Laws*. 2017:211-38. <https://doi.org/10.48550/arXiv.1607.05514>
- [13] Keller-Ressel M, Nargang S. The hyperbolic geometry of financial networks. *Scientific reports*. 2021 Feb 26;11(1):4732. <https://doi.org/10.1038/s41598-021-83328-4>

- [14] García-Pérez G, Boguñá M, Allard A, Serrano MÁ. The hidden hyperbolic geometry of international trade: World Trade Atlas 1870–2013. *Scientific reports*. 2016 Sep 16;6(1):33441. <https://doi.org/10.1038/srep33441>
- [15] Muscoloni A, Thomas JM, Ciucci S, Bianconi G, Cannistraci CV. Machine learning meets complex networks via coalescent embedding in the hyperbolic space. *Nature communications*. 2017 Nov 20;8(1):1615. <https://doi.org/10.1038/s41467-017-01825-5>
- [16] Cacciola A, Muscoloni A, Narula V, Calamuneri A, Nigro S, Mayer EA, Labus JS, Anastasi G, Quattrone A, Quartarone A, Milardi D. Coalescent embedding in the hyperbolic space unsupervisedly discloses the hidden geometry of the brain. *arXiv preprint arXiv:1705.04192*. 2017 May 10. <https://doi.org/10.48550/arXiv.1705.04192>
- [17] Zhou Y, Sharpee TO. Hyperbolic geometry of gene expression. *Iscience*. 2021 Mar 19;24(3). <https://doi.org/10.1016/j.isci.2021.102225>
- [18] Keller-Ressel M, Nargang S. Hydra: a method for strain-minimizing hyperbolic embedding of network-and distance-based data. *Journal of Complex Networks*. 2020 Feb;8(1):cnaa002. <https://doi.org/10.48550/arXiv.1903.08977>
- [19] García-Pérez G, Allard A, Serrano MÁ, Boguñá M. Mercator: uncovering faithful hyperbolic embeddings of complex networks. *New Journal of Physics*. 2019 Dec 1;21(12):123033. <https://doi.org/10.1088/1367-2630/ab57d2>
- [20] Krioukov D, Papadopoulos F, Kitsak M, Vahdat A, Boguñá M. Hyperbolic geometry of complex networks. *Physical Review E*. 2010 Sep 9;82(3):036106. <https://doi.org/10.1103/PhysRevE.82.036106>
- [21] Loustau B. Hyperbolic geometry. *arXiv e-prints*. 2020 Mar:arXiv-2003. <https://doi.org/10.48550/arXiv.2003.11180>
- [22] Newman ME. Fast algorithm for detecting community structure in networks. *Physical review E*. 2004 Jun 18;69(6):066133. <https://doi.org/10.1103/PhysRevE.69.066133>

- [23] Tenenbaum JB, Silva VD, Langford JC. A global geometric framework for nonlinear dimensionality reduction. *science*. 2000 Dec 22;290(5500):2319-23. <https://doi.org/10.1126/science.290.5500.2319>
- [24] Danon L, Diaz-Guilera A, Duch J, Arenas A. Comparing community structure identification. *Journal of statistical mechanics: Theory and experiment*. 2005 Sep 26;2005(09):P09008. <https://doi.org/10.1088/1742-5468/2005/09/P09008>
- [25] Danon L, Diaz-Guilera A, Arenas A. The effect of size heterogeneity on community identification in complex networks. *Journal of Statistical Mechanics: Theory and Experiment*. 2006 Nov 15;2006(11):P11010. <https://doi.org/10.1088/1742-5468/2006/11/P11010>
- [26] Nickel M, Kiela D. Poincaré embeddings for learning hierarchical representations. *Advances in neural information processing systems*. 2017;30.
- [27] <https://github.com/AlexPof/PoincareKMeans>
- [28] Vinh NX, Epps J, Bailey J. Information theoretic measures for clusterings comparison: is a correction for chance necessary?. In *Proceedings of the 26th annual international conference on machine learning 2009 Jun 14* (pp. 1073-1080).
- [29] Muscoloni A, Cannistraci CV. Angular separability of data clusters or network communities in geometrical space and its relevance to hyperbolic embedding. *arXiv preprint arXiv:1907.00025*. 2019 Jun 28. <https://doi.org/10.48550/arXiv.1907.00025>.
- [30] Serrano MÁ, Krioukov D, Boguná M. Self-similarity of complex networks and hidden metric spaces. *Physical review letters*. 2008 Feb 20;100(7):078701.
- [31] Boguná M, Pastor-Satorras R. Class of correlated random networks with hidden variables. *Physical Review E*. 2003 Sep 15;68(3):036112. <https://doi.org/10.1103/PhysRevE.68.036112>
- [32] Prim RC. Shortest connection networks and some generalizations. *The Bell System Technical Journal*. 1957 Nov;36(6):1389-401. <https://doi.org/10.1002/j.1538-7305.1957.tb01515.x>

- [33] Boyer JM, Myrvold WJ. Simplified $O(n)$ planarity by edge addition. *Graph Algorithms Appl.* 2006 Jun 14;5:241. https://doi.org/10.1142/9789812773289_0014
- [34] Euler L. *Elementa doctrinae solidorum. Novi commentarii academiae scientiarum Petropolitanae.* 1758:109-40.
- [35] Chrobak M, Payne TH. A linear-time algorithm for drawing a planar graph on a grid. *Information Processing Letters.* 1995 May 26;54(4):241-6. [https://doi.org/10.1016/0020-0190\(95\)00020-D](https://doi.org/10.1016/0020-0190(95)00020-D)
- [36] István F. On straight-line representation of planar graphs. *Acta scientiarum mathematicarum.* 1948;11(229-233):2.
- [37] Clauset A, Shalizi CR, Newman ME. Power-law distributions in empirical data. *SIAM review.* 2009;51(4):661-703. <https://doi.org/10.1137/070710111>
- [38] Kovács B, Palla G. The inherent community structure of hyperbolic networks. *Scientific Reports.* 2021 Aug 6;11(1):16050. <https://doi.org/10.1038/s41598-021-93921-2>
- [39] Belkin M, Niyogi P. Laplacian eigenmaps for dimensionality reduction and data representation. *Neural computation.* 2003 Jun 1;15(6):1373-96. <https://doi.org/10.1162/089976603321780317>
- [40] Cannistraci CV, Alanis-Lobato G, Ravasi T. Minimum curvilinearity to enhance topological prediction of protein interactions by network embedding. *Bioinformatics.* 2013 Jul 1;29(13):i199-209. <https://doi.org/10.1093/bioinformatics/btt208>
- [41] Cannistraci CV, Ravasi T, Montecchi FM, Ideker T, Alessio M. Nonlinear dimension reduction and clustering by Minimum Curvilinearity unfold neuropathic pain and tissue embryological classes. *Bioinformatics.* 2010 Sep 15;26(18):i531-9. <https://doi.org/10.1093/bioinformatics/btq376>

- [42] Dorogovtsev SN, Mendes JF, Samukhin AN. Structure of growing networks with preferential linking. *Physical review letters*. 2000 Nov 20;85(21):4633. <https://doi.org/10.1103/PhysRevLett.85.4633>
- [43] Wang J, Wang J. *Geometric structure of high-dimensional data*. Springer Berlin Heidelberg; 2012. <https://doi.org/10.1007/978-3-642-27497-8>
- [44] Liu R, Cai H, Luo C. Clustering analysis of stocks of csi 300 index based on manifold learning. *Journal of Intelligent Learning Systems and Applications*. 2012 May 23;4(02):120-6. <http://dx.doi.org/10.4236/jilsa.2012.42011>
- [45] Dijkstra EW. A note on two problems in connexion with graphs. In *Edsger Wybe Dijkstra: His Life, Work, and Legacy* 2022 Jul 12 (pp. 287-290). <https://doi.org/10.1145/3544585.3544600>
- [46] Zar JH. *Biostatistical analysis*. Pearson Education India; 1999.
- [47] Bollinger J. *Bollinger on Bollinger bands*. New York: McGraw-Hill; 2002.

Table 1: Price statistics of CNX100 Index of the year 2020 and 2018.

Years	Min	Mean	Max	Standard deviation
2018	10307.70	11045.40	12028.29	367.52
2020	7719.10	11326.20	14090.75	1388.96

Table 2: Healthy period and Crisis period MST networks topological properties.

Years	Weighted mean degree (MD)	Average shortest path distance (SD)	Average local clustering coefficient (CC)	Average edge weight (EW)
2018	0.9292	6.0995	0	0.4658
2020	1.0210	7.7720	0	0.5118

The rows 2 to 6 of the table 3 and Table 4 gives the NMI (or AMI) score between the \mathcal{C}^{top} and \mathcal{C}^{Euc} , and next rows 7 to 11 gives the NMI (or AMI) score between the \mathcal{C}^{top} and \mathcal{C}^{hyp} . EA is equidistance adjustment and CA is circular adjustment. The results are similar for EA and CA, so we only present for EA case.

Table 3: NMI Scores: $NMI(\mathcal{C}^{top}, \mathcal{C}^{Euc})$ and $NMI(\mathcal{C}^{top}, \mathcal{C}^{hyp})$.

Methods	2017	2018	2019	2020	2021
ISO	0.693	0.695	0.683	0.746	0.779
ncISO	0.608	0.583	0.649	0.659	0.688
LE	0.141	0.116	0.135	0.121	0.148
MCE	0.694	0.694	0.676	0.751	0.78
ncMCE	0.604	0.584	0.644	0.66	0.693
Coal-ISO-EA	0.705	0.677	0.641	0.683	0.826
Coal-ncISO-EA	0.698	0.579	0.644	0.668	0.797
Coal-LE-EA	0.795	0.772	0.752	0.817	0.854
Coal-MCE-EA	0.592	0.602	0.631	0.639	0.685
Coal-ncMCE-EA	0.619	0.72	0.702	0.791	0.811

Table 4: AMI Scores: $AMI(\mathcal{C}^{top}, \mathcal{C}^{Euc})$ and $AMI(\mathcal{C}^{top}, \mathcal{C}^{hyp})$.

Methods	2017	2018	2019	2020	2021
ISO	0.625	0.653	0.623	0.702	0.744
ncISO	0.519	0.525	0.582	0.598	0.638
LE	0.005	0.017	0.019	0.023	0.041
MCE	0.628	0.654	0.615	0.707	0.746

ncMCE	0.516	0.528	0.575	0.6	0.643
Coal-ISO-EA	0.637	0.632	0.57	0.625	0.799
Coal-ncISO-EA	0.628	0.522	0.574	0.607	0.764
Coal-LE-EA	0.748	0.741	0.703	0.784	0.831
Coal-MCE-EA	0.502	0.547	0.558	0.575	0.634
Coal-ncMCE-EA	0.535	0.681	0.643	0.752	0.78

Table 5: NMI dynamics of NMI_{top}^{hyp} and NMI_{top}^{Euc} for MST network.

Methods	mean NMI_{top}^{hyp}	mean NMI_{top}^{Euc}	p -value
ISO, Coal-ISO-EA	0.654	0.698	1
ncISO, Coal-ncISO-EA	0.655	0.594	3.27297878e-75
LE, Coal-LE-EA	0.766	0.121	7.86206154e-289
MCE, Coal-MCE-EA	0.585	0.698	1
ncMCE, Coal-ncMCE-EA	0.659	0.595	8.36831297e-77

Table 6: Healthy period versus Crisis period: Mann Whitney Test p -values.

Methods	mean measure crisis period (year 2020)	mean measure healthy period (year 2018)	p -value
ISO-CA-HD	20.13	19.77	2.71E-06
ISO-CA-HSD	152.80	115.41	0.00E+00
ISO-EA-HD	21.311	21.03	8.40E-10
ISO-EA-HSD	180.39	140.20	0.00E+00
ncISO- CA-HD	20.41	20.03	1.18E-07

ncISO- CA-HSD	164.36	124.92	0.00E+00
ncISO-EA-HD	21.31	21.03	8.44E-10
ncISO-EA-HSD	180.36	141.05	0.00E+00
LE- CA-HD	20.13	19.62	3.40E-08
LE- CA-HSD	138.29	99.01	0.00E+00
LE-EA-HD	21.311	21.03	8.57E-10
LE-EA-HSD	173.36	133.80	0.00E+00
MCE- CA-HD	20.44	20.15	4.12E-10
MCE- CA-HSD	173.57	138.25	0.00E+00
MCE-EA-HD	21.31	21.03	8.44E-10
MCE-EA-HSD	182.64	144.34	0.00E+00
ncMCE- CA-HD	20.44	20.03	6.29E-08
ncMCE- CA-HSD	173.57	131.94	0.00E+00
ncMCE-EA-HD	21.31	21.03	8.53E-10
ncMCE-EA-HSD	182.64	142.48	0.00E+00
Average EW	0.2879	0.2759	0.2633
Average SD	9.6609	8.0407	1.11E-14

In Table 6. HD represent the hyperbolic distance and HSD represent the hyperbolic shortest path distance. EA represents the Equidistance adjustment and CA represents the circular adjustment. EW is edge weight and SD is shortest path distance of original network.

Table 7: ASI index score for the topological communities.

Methods	2017	2018	2019	2020	2021

ISO-EA	0.8588	0.8725	0.8449	0.8776	0.9620
ncISO-EA	0.8882	0.7991	0.8637	0.8720	0.9447
LE-EA	0.9683	0.9694	0.9490	0.9776	0.9770
MCE-EA	0.8001	0.8307	0.8520	0.8614	0.8903
ncMCE-EA	0.7750	0.9237	0.9179	0.9547	0.9671

In Table 7. EA represent the equidistance adjustment. The results are similar for EA and CA, so we present only for EA.

Fig 1: Price trend of CNX100 index for year 2018 and year 2020.

(a) Year 2018 Healthy period. b) Year 2020 Crisis period.

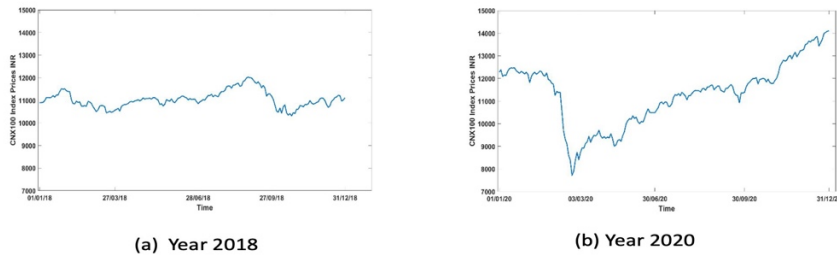


Fig 2: Embedded networks (2017 data)

a) MST network. b) MST network embedded in Euclidean plane via Isomap. c) MST network embedded in Poincare disc via coalescent embedding (ISO-EA). d) MST network embedded in Poincare disc via coalescent embedding (ISO-CA). Different colours represent different communities in \mathcal{C}^{top} .

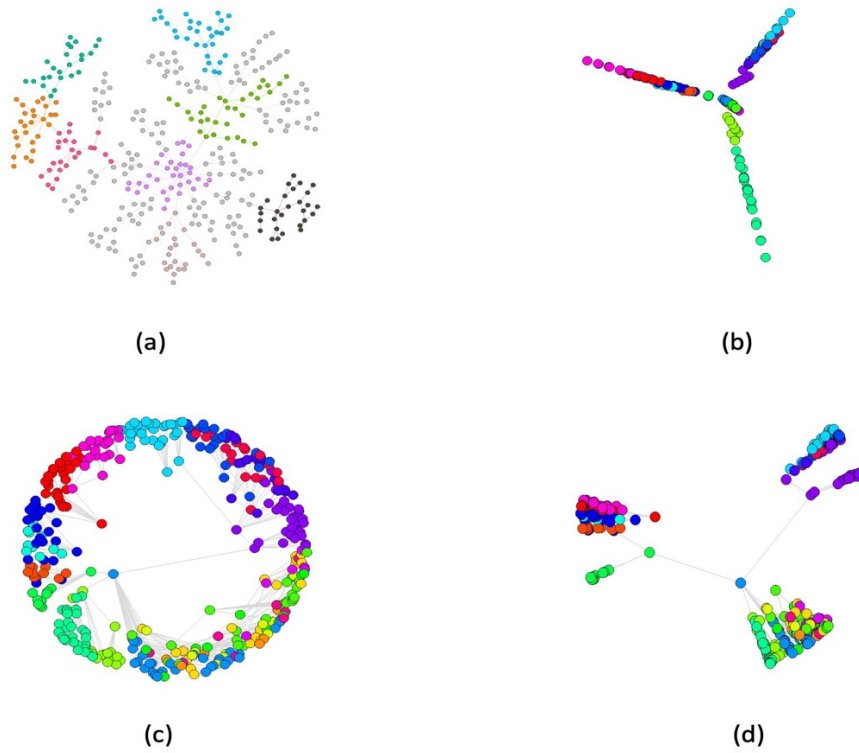
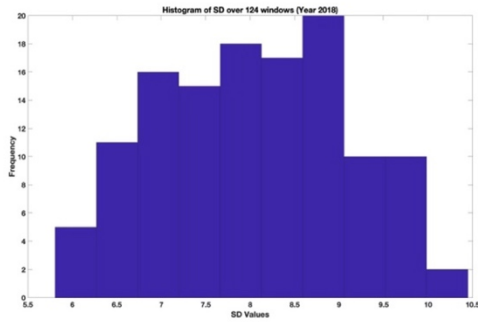
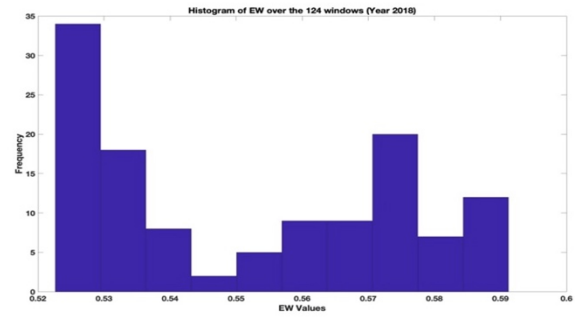


Fig. 3. Probability distribution of the mean measures as depicted in histogram of the original as well as embedded network (ISO-EA) for healthy period year 2018.

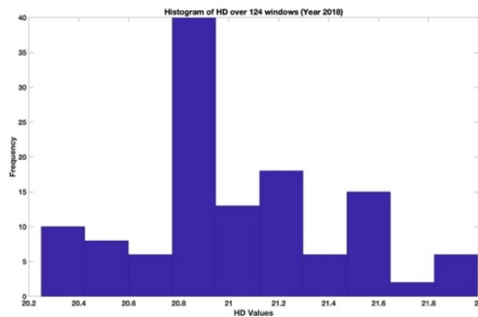
These probability distributions do not exhibit a power-law distribution as mentioned lower p -value with their measure name; a). Shortest path distance (SD) ($1.639108e-08$) b). Edge weight (EW) (0.0009421079) c). Hyperbolic distance (HD) ($1.2702e-17$) d). Hyperbolic shortest path distance (HSD) ($1.638783e-12$).



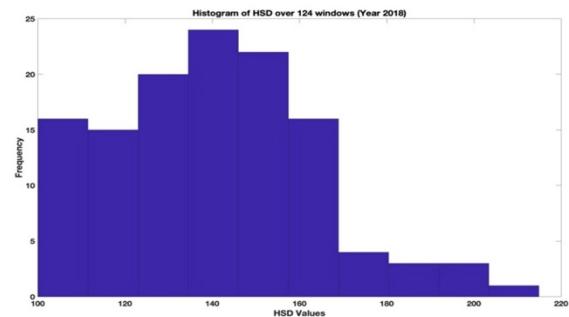
a) SD



b) EW



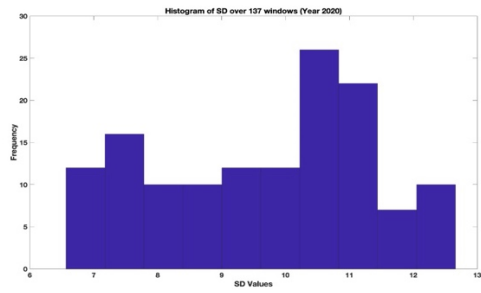
c) HD



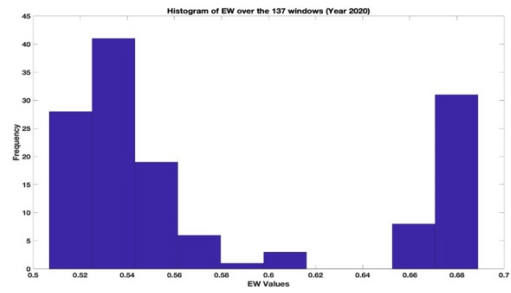
d) HSD

Fig. 4. Probability distribution of the mean measures as depicted in histogram of the original as well as embedded network (ISO-EA) for crisis period year 2020.

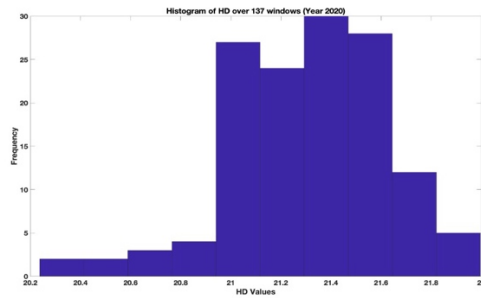
These probability distributions do not exhibit a power-law distribution as mentioned lower p -value with their measure name; a). Shortest path distance (SD) ($9.558699e-07$) b). Edge weight (EW) (0.0008558102) c). Hyperbolic distance (HD) ($2.56657e-14$) d). Hyperbolic shortest path distance (HSD) ($1.716373e-14$).



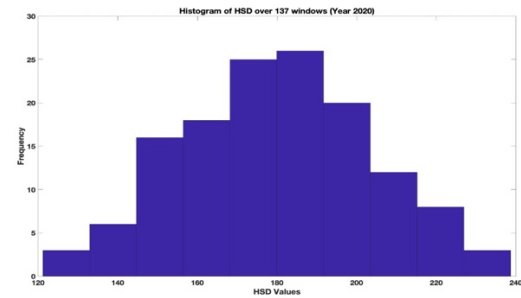
a) SD



b) EW



a) HD



b) HSD

Fig 5: BB analysis on original modularity

lowerBB (blue), middleBB (orange) and upperBB (grey).

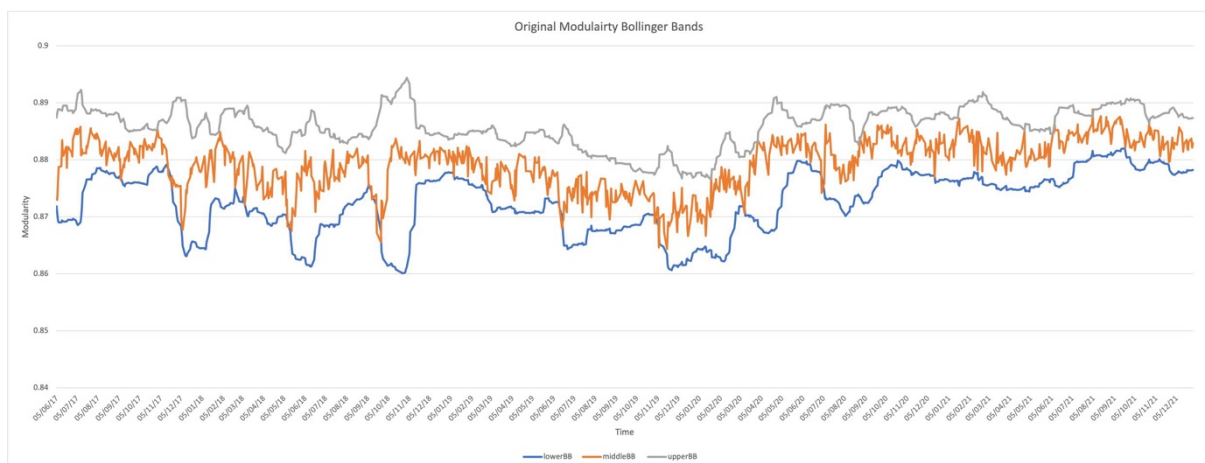


Fig 6: BB analysis on hyperbolic modularity

lowerBB (blue), middleBB (orange) and upperBB (grey).

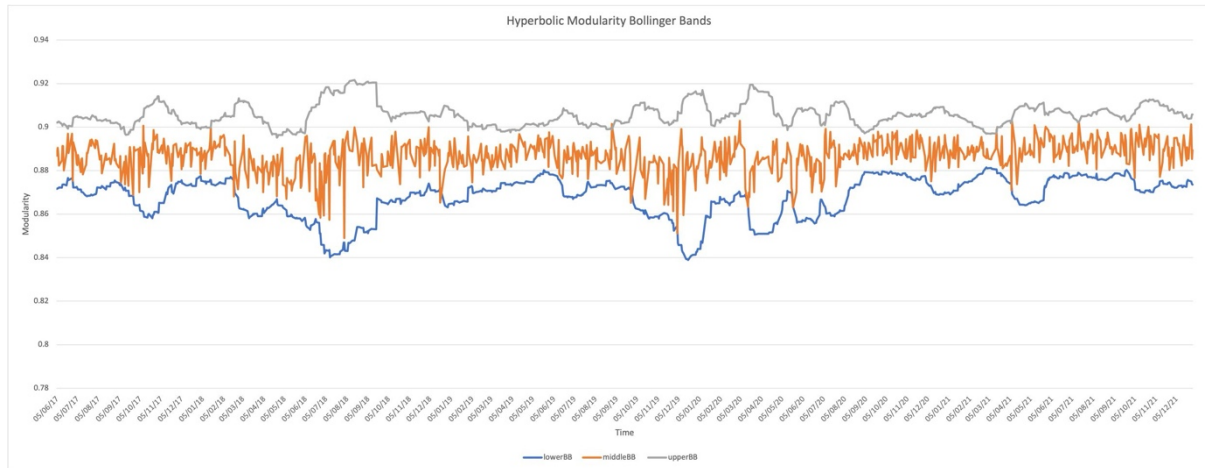


Fig 7: BB analysis on CNX100 prices.

lowerBB (blue), middleBB (orange) and upperBB (grey).

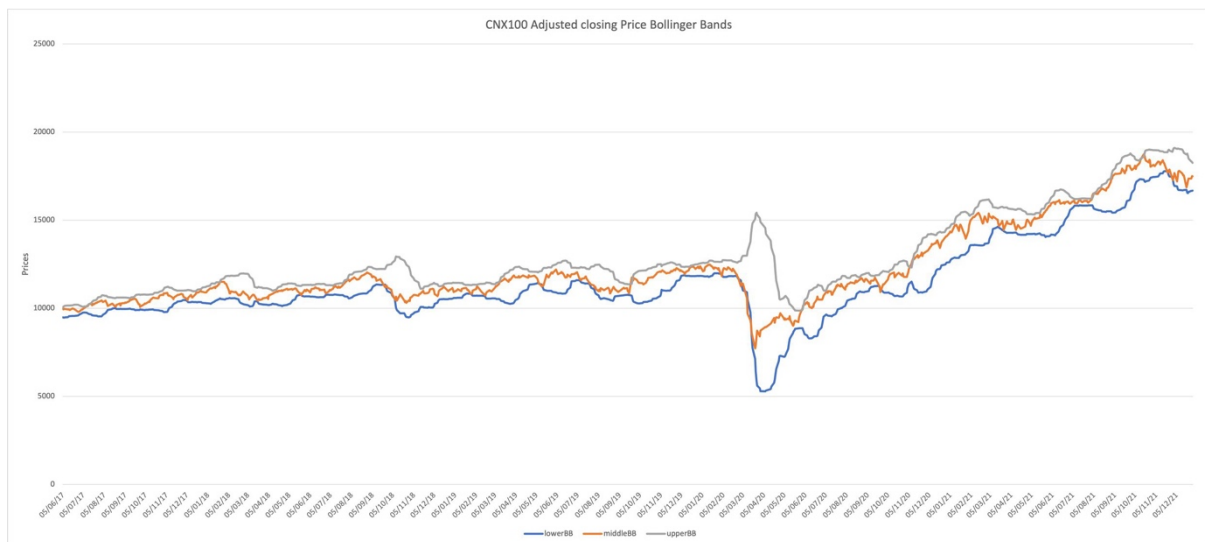


Fig 8: Plot of the coalescent embedding Poincare disc.

(a) ISO-EA (b) ISO-CA for the sectors: Finance (red) and Healthcare (cyan).

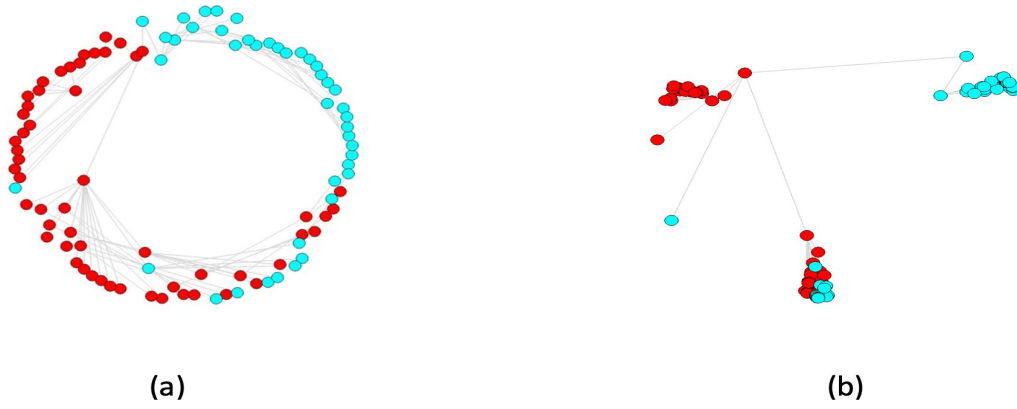
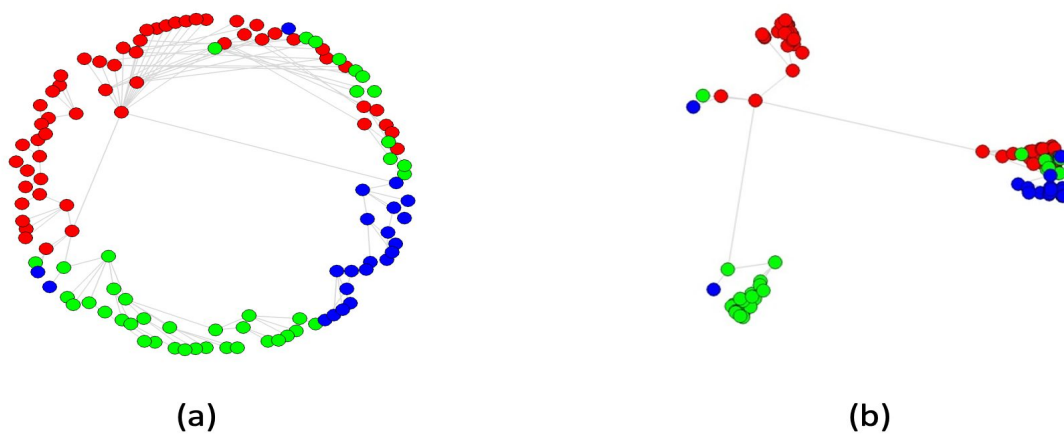


Fig 9: Plot of the coalescent embedding in Poincare disc.

(a) ISO-EA (b) ISO-CA for the sectors: Finance (Red), Healthcare (green), and Information technology (blue).

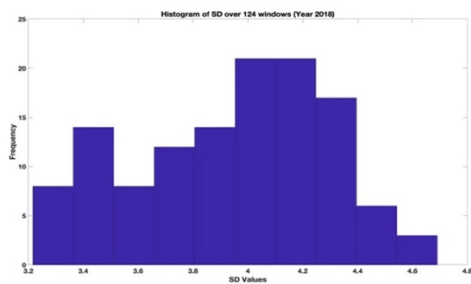


Supporting Information

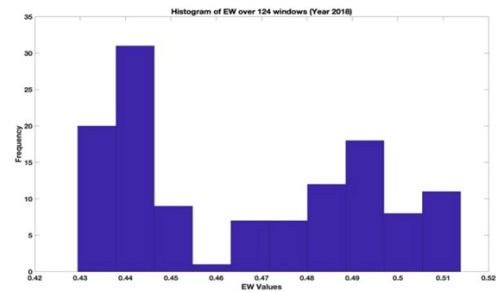
S1 Fig (a) and (b). Probability distribution of the mean measures as depicted in histogram for the PMFG network corresponding to both the periods.

S1 Fig. a). Probability distribution of the mean measures as depicted in histogram of the original as well as embedded network (ISO-EA) for healthy period year 2018 of PMFG network.

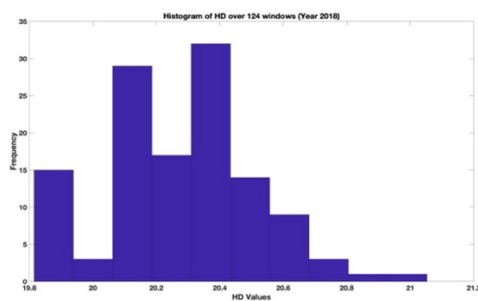
These probability distributions do not exhibit a power-law distribution as mentioned lower p -value with their measure name; a). Shortest path distance (SD) ($1.965097e-07$) b). Edge weight (EW) (0.003234001) c). Hyperbolic distance (HD) ($6..676684e-09$) d). Hyperbolic shortest path distance (HSD) ($6.204048e-11$).



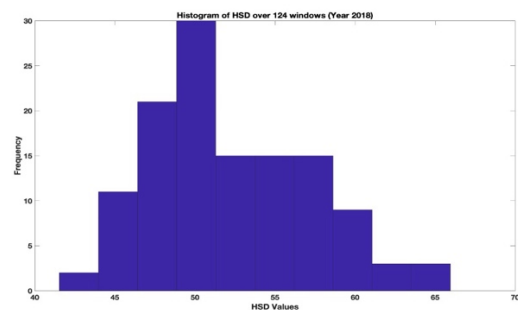
a) SD



b) EW

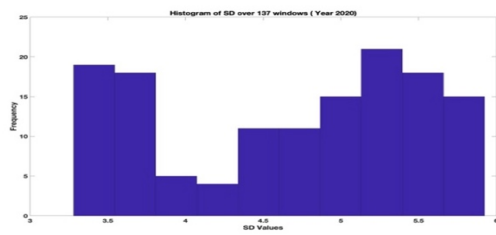


c) HD

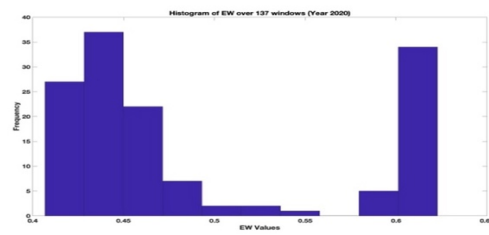


d) HSD

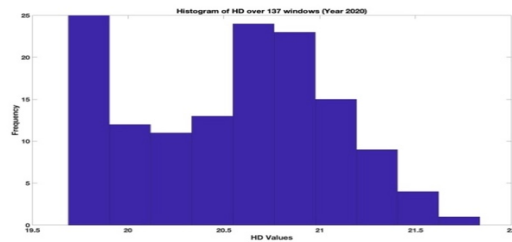
S1 Fig. b). Probability distribution of the mean measures as depicted in histogram of the original as well as embedded network (ISO-EA) for crisis period year 2020 of PMFG network. These probability distributions do not exhibit a power-law distribution as mentioned lower p -value with their measure name; a). Shortest path distance (SD) ($1.965097e-07$) b). Edge weight (EW) (0.003234001) c). Hyperbolic distance (HD) ($6..676684e-09$) d). Hyperbolic shortest path distance (HSD) ($6.204048e-11$).



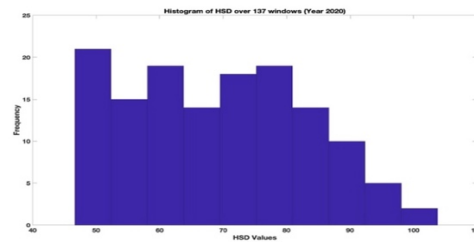
a) SD



b) EW



a) HD



b) HSD

S1 Table. Estimated power law exponent γ of the degree distribution of networks.

Year	MST - Power-law coefficient γ (p -value)	PMFG - Power-law coefficient γ (p -value)	PTN - Power-law coefficient γ (p -value)
2017	2.706 (0.355)	2.575 (0.931)	2.274 (0.555)
2018	2.687 (0.999)	2.657 (0.699)	2.327 (1.78E-35)
2019	2.718 (0.449)	2.613 (0.990)	2.302 (0.00E+00)
2020	2.638 (0.111)	2.576 (0.994)	2.294 (0.897)
2021	2.880 (0.164)	2.505 (0.176)	2.225 (8.58E-33)

S2 Table : Healthy period and Crisis period PMFG networks topological properties.

Years	Weighted mean degree (MD)	Average shortest Path distance (SD)	Average local clustering coefficient (CC)	Average edge weight (EW)
2018	2.4214	3.4988	0.7674	0.4057
2020	2.6909	3.8404	0.7499	0.4508

S3 Table (a): NMI Scores: $NMI(\mathcal{C}^{top}, \mathcal{C}^{Euc})$ and $NMI(\mathcal{C}^{top}, \mathcal{C}^{hyp})$ for PMFG Network

Methods	2017	2018	2019	2020	2021
ISO	0.6004	0.5531	0.7299	0.6601	0.6852
ncISO	0.4507	0.4395	0.5870	0.5085	0.4842
LE	0.0701	0.0739	0.0481	0.0861	0.0607
MCE	0.6128	0.5363	0.6198	0.6509	0.7014
ncMCE	0.5445	0.4156	0.6256	0.5953	0.6309
Coal-ISO-EA	0.5750	0.5482	0.6857	0.6253	0.6268
Coal-ncISO-EA	0.5940	0.5723	0.5927	0.6263	0.6336
Coal-LE-EA	0.6806	0.6070	0.6184	0.6661	0.7504
Coal-MCE-EA	0.4849	0.4438	0.5144	0.5405	0.5765
Coal-ncMCE-EA	0.5226	0.5313	0.5674	0.6765	0.6808

S3 Table (b): AMI Scores: $AMI(\mathcal{C}^{top}, \mathcal{C}^{Euc})$ and $AMI(\mathcal{C}^{top}, \mathcal{C}^{hyp})$ for PMFG Network.

Methods	2017	2018	2019	2020	2021
ISO	0.5819	0.5199	0.7239	0.6364	0.6713
ncISO	0.4252	0.3978	0.5786	0.4743	0.4609
LE	0.0186	0.0127	0.0168	0.0212	0.0091
MCE	0.5943	0.5026	0.6120	0.6267	0.6879
ncMCE	0.5231	0.3729	0.6173	0.5674	0.6145
Coal-ISO-EA	0.5565	0.5158	0.6794	0.5993	0.6099
Coal-ncISO-EA	0.5762	0.5411	0.5847	0.6022	0.6180
Coal-LE-EA	0.6666	0.5783	0.6110	0.6440	0.7397
Coal-MCE-EA	0.4620	0.4039	0.5049	0.5093	0.5584
Coal-ncMCE-EA	0.5018	0.4986	0.5591	0.6545	0.6673

S4 Table. NMI dynamics of NMI_{top}^{hyp} and NMI_{top}^{Euc} for PMFG network.

Methods	mean NMI_{top}^{hyp}	mean NMI_{top}^{Euc}	p -value
ISO, Coal-ISO-EA	0.5562	0.6252	1
ncISO, Coal-ncISO-EA	0.5576	0.4947	5.00774697e-74
LE, Coal-LE-EA	0.6345	0.0635	7.86206154e-289
MCE, Coal-MCE-EA	0.4706	0.5992	1
ncMCE, Coal-ncMCE-EA	0.5217	0.4874	1.18882772e-18

S5 Table. Healthy period versus Crisis period: Mann Whitney Test p -values for PMFG networks.

Methods	Mean Measure Crisis Period (Year 2020)	Mean Measure Healthy Period (Year 2018)	<i>p</i> -value
ISO-CA-HD	19.77301	19.72157	1.41E-01
ISO-CA-HSD	59.55195	46.08662	0.00E+00
ISO-EA-HD	20.55894	20.27156	6.45E-07
ISO-EA-HSD	69.18347	52.31449	0.00E+00
ncISO-CA-HD	19.90197	19.77596	6.60E-03
ncISO-CA-HSD	63.57935	48.49871	0.00E+00
ncISO-EA-HD	20.55894	20.27156	6.29E-07
ncISO-EA-HSD	70.44252	53.54735	0.00E+00
LE-CA-HD	19.61113	19.41034	2.45E-03
LE-CA-HSD	56.95834	43.65652	0.00E+00
LE-EA-HD	20.55894	20.27156	6.03E-07
LE-EA-HSD	68.84244	52.37834	0.00E+00
MCE-CA-HD	19.9156	19.38465	3.11E-10
MCE-CA-HSD	67.04745	50.91291	0.00E+00
MCE-EA-HD	20.55894	20.27156	4.08E-07
MCE-EA-HSD	71.5531	55.47197	0.00E+00
ncMCE-CA-HD	19.69202	19.26732	3.02E-08
ncMCE-CA-HSD	63.81771	48.26688	0.00E+00
ncMCE-EA-HD	20.55894	20.27156	4.55E-07
ncMCE-EA-HSD	70.8716	54.8257	0.00E+00
Average (EW)	0.4907	0.4657	0.33622
Average SD	4.6804	3.9469	4.1072e-12

S6 Table. ASI Score for topological communities of PMFG network.

Methods	2017	2018	2019	2020	2021
ISO-EA	0.745534	0.69326	0.72188	0.804965	0.777182
ncISO-EA	0.756806	0.733355	0.730274	0.807613	0.820136
LE-EA	0.855997	0.791137	0.814732	0.881431	0.879758
MCE-EA	0.557049	0.537714	0.629692	0.746074	0.736861
ncMCE-EA	0.617045	0.63987	0.626749	0.822581	0.803692